Earthquakes and Structures, *Vol. 17, No. 2 (2019) 163-173*
DOI: https://doi.org/10.12989/eas.2019.17.2.163

Cyclic testing of scaled three-story special concentrically braced frame with strongback column

Chui-Hsin Chen*, Yi-Rung Tsai[a] and Yao Tang[b]

Department of Civil Engineering, National Chiao Tung University, 1001 University Rd. Hsinchu 30010, Taiwan

(Received February 21, 2019, Revised April 15, 2019, Accepted May 8, 2019)

Abstract. For Special Concentrically Braced Frame (SCBF), it is common that the damage concentrates at a certain story instead of spreading over all stories. Once the damage occurs, the soft-story mechanism is likely to take place and possibly to result in the failure of the whole system with more damage accumulation. In this study, we use a strongback column which is an additional structural component extending along the height of the building, to redistribute the excessive deformation of SCBF and activate more structural members to dissipate energy and thus avoid damage concentration and improve the seismic performance of SCBF. We tested one-third-scaled, three-story, double-story X SCBF specimens with static cyclic loading procedure. Three specimens, namely S73, S42 and S0, which represent different combinations of stiffness and strength factors α and β for the strongback columns, were designed based on results of numerical simulations. Specimens S73 and S42 were the specimens with the strongback columns, and S0 is the specimen without the strongback column. Test results show that the deformation distribution of Specimen S73 is more uniform and more brace members in three stories perform nonlinearly. Comparing Drift Concentration Factor (DCF), we can observe 29% and 11% improvement in Specimen S73 and S42, respectively. This improvement increases the nonlinear demand of the third-story braces and reduces that of the first-story braces where the demand used to be excessive, and, therefore, postpones the rupture of the first-story braces and enhances the ductility and energy dissipation capacity of the whole SCBF system.

Keywords: special concentrically braced frame; soft story; strongback column; static cyclic loading; drift concentration factor; energy dissipation capacity

1. Introduction

Special concentrically braced frame (SCBF) system is one of the most common structural systems worldwide because of its efficiency to provide lateral strength and stiffness to the structures. Steel braces are also commonly used for retrofitting (Güneyisi and Azez 2016, Tehranizadeh *et al*. 2016) or working together (Eskandari *et al*. 2017) with other structural systems. However, under large earthquake excitations, the braces suffer from buckling and rupture, which usually result in a significant reduction of the strength and stiffness at a certain story. Therefore, the soft-story mechanism is likely to occur in SCBF structures (as shown in Fig. 1) and causes permanent damage or collapse of the structures (Uriz and Mahin 2008, Chen and Mahin 2012). Previous research efforts (Tremblay 2003, Tremblay and Merzouq 2004, Simpson and Mahin 2018, Pollino *et al*. 2017, Qu *et al*. 2014, Qu *et al*. 2015, Qu *et al*. 2016) used relative elastic truss structures incorporating with SCBF or buckling restrained braced frame (BRBF) to create uniformly deformed structures. Related tests were conducted by Slovenec *et al*. (2017). They tested two 3-story specimens representing a non-seismic detailed CBF with a 3-story stiff rocking core (SRC) and a 6-story SCBF with 2-story SRC. Hybrid simulation was used to investigate the fundamental behavior of the SRC rehabilitation technique and to explore its practical design challenges. A similar method was proposed by using stiff members, i.e., strongbacks, to improve the tendency to form the unfavorable soft-story mechanism. The behavior of hybrid strongback system which applied to a zipper-frame configuration (Khatib *et al*. 1988, Sabelli 2001, Tirca and Tremblay 2004) was investigated numerically (Lai and Mahin 2013). Such an idea of keeping half bay to remain elastic and work as an elastic frame or a strongback has been applied to real practice (Mar 2010). Similar to the idea of strongback, other research (MacRae *et al*. 2004) considered the contributions of gravity columns to lateral force resistance and concluded that the gravity columns were able to reduce the deformation concentration. Further study (Ji *et al*. 2009) quantitatively investigated the effects of continuous gravity columns on braced frame structures and concluded that a sufficient number of gravity columns reduced the deformation concentration effectively. More recently, a successful application of strongback concept employed post-tensioned rocking walls, which played the role of strongback, with shear dampers to improve the energy dissipation mechanism of a moment resisting frame building (Wada *et al*. 2011, Qu *et al*. 2012).

*Corresponding author, Assistant Professor
E-mail: chence@nctu.edu.tw
[a]Graduate Student Researcher
E-mail: a0917912038@gmail.com
[b]Graduate Student Researcher
E-mail: yao771124.cv96@g2.nctu.edu.tw

http://www.techno-press.com/journals/eas&subpage=7
ISSN: 2092-7614 (Print), 2092-7622 (Online)

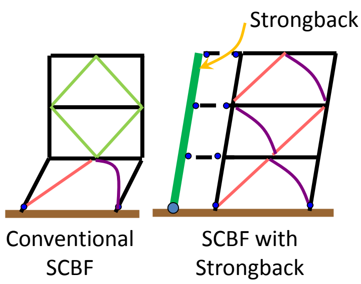

Fig. 1 The improvement of soft-story mechanism in SCBF by utilizing the strongback

The design parameters of the strongback system are still under development. More experimental and analytical investigations are required. The objectives of this study are to validate the effectiveness of the strongback, to identify possible failure modes of the strongback system through experiments, and to quantify the design parameters of strongback system for its application to SCBF structures. We investigate how the strength and stiffness of the strongback system affect the global behavior of SCBF frame in this study. There is no specific form of the strongback. To simplify the structural behavior, we used a column to represent the strongback components in the current study. Through experiments, we looked into the effects of the strongback column on the failure modes, drift ratio, energy dissipation, and drift concentration factor (DCF) which was defined as DRmax/DRavg (maximum drift ratio/ roof drift ratio) (MacRae *et al*. 2004).

2. Design of specimens

The design of the specimens was based on the previous numerical study (Chen *et al*. 2016) where a series of nonlinear dynamic and static analyses were conducted to investigate the effects of the strongback column on the system behavior of SCBF.

2.1 Design parameters (stiffness factor, strength factor)

The strongback column should be designed based on certain criteria of structural design. Stiffness and strength are the two most important parameters for structural design. Therefore, we choose stiffness and strength as the design parameters to design the strongback column. This study uses stiffness factor (α) and strength factor (β) to represent the relationship between the strongback column and concentrically braced frame.

We define α as the ratio of the lateral stiffness of the strongback column to the horizontal stiffness contributed from braces at the first story, and is expressed in Eq. (1). We define β as the ratio of the lateral strength of the strongback column to the horizontal strength contributed from braces at the first story, and is expressed in Eq. (2).

$$\alpha = \frac{(EI/h^3)_{strongback}}{K_{h,brace}} \tag{1}$$

$$\beta = \frac{M_{PS}/h}{(R_y P_y + 0.3P_{cr})\cos\varphi} \tag{2}$$

where E is Young's modulus of steel, I is the moment of inertia of the strongback column, h is the story height, $K_{h,brace}$ is the horizontal stiffness contributed from only braces in a story, M_{PS} is the moment capacity of the strongback column, R_y is overstrength factor of steel (AISC 2010), P_y is the yielding strength of a brace, P_{cr} is the compression strength of a brace and φ is the incline angle of the brace with respect to horizon in the frame. The calculation of $K_{h,brace}$ is based on the summation of the axial stiffness of the braces; providing a simple and accurate estimation, it is appropriate to form a basis to define stiffness factor. The denominator of strength factor is based on the horizontal components of the braces in the chevron configuration. It accounts for the limit condition that one brace is in tension and the other is in compression after the brace severely buckles. The tension brace develops the tension strength up to R_yP_y while the compression brace sustains the capacity of $0.3P_{cr}$. To make the strength factor dimensionless, we use a term of force in the numerator. A special case of α factor and β factor is taking the sizes of a column in the frame as those of the strongback column; the corresponding α factor is 0.0024 and β is 0.027.

2.2 Numerical simulations for specimen design

OpenSEEs was employed to simulate the nonlinear behavior of the three-story SCBF. The structures were simulated with a two-dimensional plane frame and a leaning column, and some were simulated with an additional continuous strongback column. In the numerical models, the columns of the frame were assumed to be continuous with the same section and fixed to the base. The beam-to-column connections were assumed to be rigid. The sectional properties of the strongback columns were the parameters to be investigated in this study.

The material model for all steel components was Menegotto-Pinto model with isotropic strain hardening (Steel02 in OpenSees). The material properties were based on previous experimental study (Uriz and Mahin 2008). To simulate the rupture behavior we adopted the rainflow cycle counting algorithm to account for the effects of low-cycle fatigue. Fiber sections were utilized for all structural components including the strongback column and gusset plates. The beams, columns and braces were modeled by using forced-based nonlinear beam-column elements. Rayleigh damping was used in the analyses with 4% damping ratio at the first-mode period (T_1) and $0.2T_1$. The numerical models have been calibrated with previous experiments (Uriz and Mahin 2008) and successfully applied in another study (Chen *et al*. 2016).

Previous numerical study (Chen *et al*. 2016) concluded that the appropriate strongback should have sufficient strength and stiffness. However, excessive strength and stiffness do not lead to the results of reducing more DCF. Numerical simulations with OpenSees (1997) were conducted to identify better stiffness factors and strength factors for design. The model structure was a three-story SCBF building with an additional column representing the

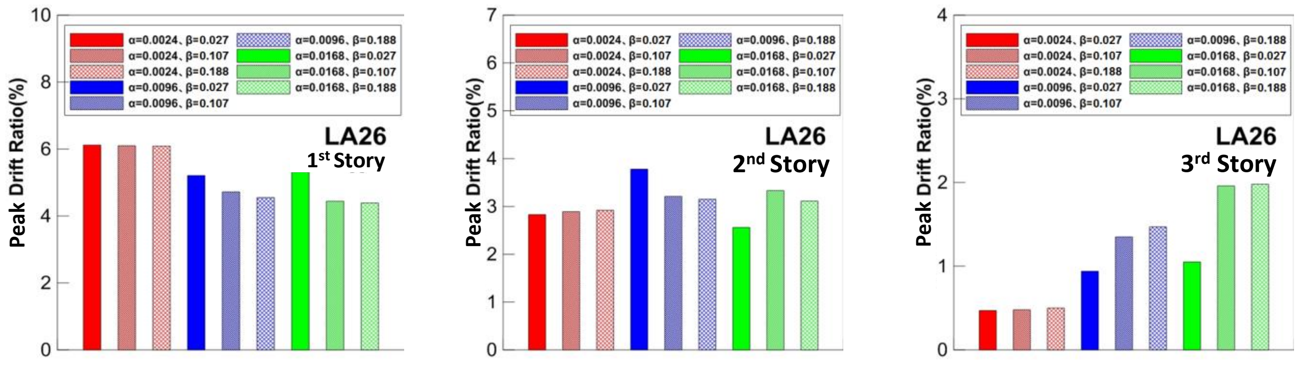

(a) (b) (c)

Fig. 2 Maximum drift ratio of three-story SCBF with various strongbacks under ground motion record LA26 (MCE-level) (a) the 1st story (b) the 2nd story (c) the 3rd story

strongback system. The original SCBF building was designed to conform to the requirements in ASCE/SEI 7-05.

Nonlinear dynamic analyses were conducted to investigate the performance of 3-story SCBF with different strength and stiffness of the strongback columns. Sixty ground motions (Somerville 1997) representing service-level earthquakes (50% probability of exceedance in 50 years, LA41 to LA60), design-level earthquakes (10% probability of exceedance in 50 years, LA01 to LA20), and MCE-level earthquakes (2% probability of exceedance in 50 years, LA21 to LA40) were applied to the buildings. The structural responses under only MCE-level earthquakes were used to design the strongback column of the test specimens.

2.2.1 Maximum drift ratio.

According to the results of numerical simulations, the strongback columns are most efficient to improve drift concentration under MCE-level earthquakes. Fig. 2 shows the maximum drift ratios at each story of three-story SCBF with various combinations of (α, β). The trend shows that increasing both α and β reduces the maximum drift ratio in the first story and redistribute the nonlinear behavior to the second and third story. For the 1st story, the maximum drift ratio reduces up to 25%; for the 2nd story, the maximum drift ratio increases about 10%; for the 3rd story, the maximum drift ratio increases about 300%. The results demonstrate that the strongback columns are effective to change the mechanism of SCBF and result in a more uniformly distributed deformation along the height of the building. As such, more structural elements in more stories will participate in dissipating input energy from earthquakes. Two of the combinations of (α, β) will be chosen for the test specimens.

2.2.2 Drift concentration factor

Fig. 3 shows the median DCF of an earthquake suite (MCE-level) corresponding to various combinations of (α, β). It shows that a strongback column with low stiffness (e.g., α=0.0024) does not reduce DCF significantly even if the strength of the strongback column is high. The strongback column is more effective when its stiffness is sufficient. On the contrary, excessive stiffness and strength

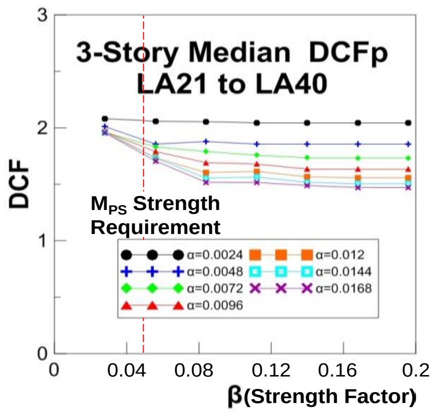

(a) Median DCFs of 3-story SCBF under MCE-level earthquakes

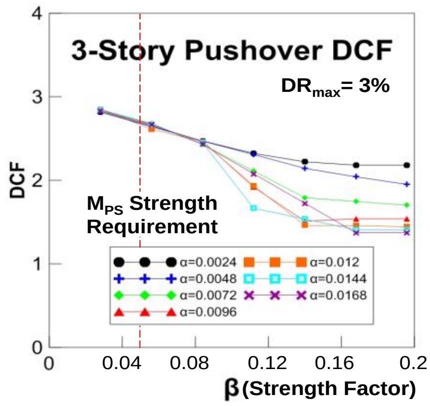

(b) DCFs of 3-story SCBF under static pushover at maximum drift ratio= 3%

Fig. 3 DCFs of 3-story SCBF subjected to dynamic and static loadings

of the strongback column (e.g., $\alpha\geq0.0096$, and $\beta\geq0.081$) cannot reduce DCF even more. Therefore, the results of analyses offer us a reference to design a strongback column with sufficient stiffness and strength without overly design it. From the case study of the numerical simulations, we will design the specimens with α in the range of $0.0096\leq\alpha\leq0.0168$ and β in the range of $0.081\leq\beta\leq0.134$. The static nonlinear analysis (Fig. 3) also gives a similar trend, although the DCF values are different. This is due to the

Table 1 Member sizes of model building and 1/3 scaled specimen

Member		Model Building (DASSE 2007)	1/3 Scaled Specimen	Scaled Factor	Scale ratio(≈3.0)
Column		W14×176	RH150×150×7×10		
		I_x = 89073 cm^4	I_x = 1620 cm^4	54.98	2.723
		I_y = 34880 cm^4	I_y = 563 cm^4	61.95	2.806
		A = 334.2 cm^2	A = 39.6 cm^2	8.44	2.905
Beam	1F	W27×84	RH198×99×4.5×7		
		I_x = 118625 cm^4	I_x = 1540 cm^4	77.03	2.963
		I_y = 4412 cm^4	I_y = 113 cm^4	39.04	2.500
		A = 160 cm^2	A = 22.7 cm^2	7.05	2.655
	2F	W30×116	RH198×150×6×9		
		I_x = 205202 cm^4	I_x = 2630 cm^4	78.02	2.972
		I_y = 6826.2 cm^4	I_y = 507 cm^4	13.46	1.915
		A = 220.6 cm^2	A = 29.9 cm^2	7.38	2.717
	3F	W36×210	RH300×150×6.5×9		
		I_x = 549425 cm^4	I_x = 7210 cm^4	76.20	2.955
		I_y = 17107 cm^4	I_y = 507 cm^4	33.74	2.410
		A = 398.7 cm^2	A = 46.8 cm^2	8.52	2.919
Brace	1F	HSS12.5×0.5	○101.6×4		
		I_x = 13277 cm^4	I_x = 146 cm^4	90.94	3.088
		A = 113.55 cm^2	A = 12.3 cm^2	9.23	3.038
		D/t = 25	D/t = 25.4	0.98	-
	2F	HSS11.25×0.5	○89.1×4		
		I_x = 9531.7 cm^4	I_x = 97 cm^4	98.26	3.148
		A = 101.94 cm^2	A = 10.7 cm^2	9.53	3.087
		D/t = 22.5	D/t = 22.3	1.00	-
	3F	HSS10×0.375	○76.3×3.2		
		I_x = 5119.64 cm^4	I_x = 49.2 cm^4	104.06	3.193
		A = 68.39 cm^2	A = 7.35 cm^2	9.30	3.050
		D/t = 26.7	D/t = 23.8	1.12	-

fact that the DCFs of the pushover analysis are calculated for the instant when the maximum drift ratio equals 3% rad. which is about the occurrence of the brace rupture and usually results in more obvious drift concentration.

2.3 Specimens (prototype frame and scaled specimens)

The SCBF specimens with the configuration of double-story X were scaled from a three-story model building designed by engineers in practice (DASSE 2007). The sizes of beam, column, and braces for the specimens were scaled with a scale ratio approximately equaled 3.0. The corresponding scale factor for cross-sectional area and moment of inertia were 9.0 and 81.0 respectively. The member sizes of model building and scaled specimen are listed in Table 1.

The effects of the composite slab were not investigated in this study, so the specimens did not include concrete slabs. Three specimens shared the same steel braced frame; the only difference between the specimens was the strongback columns. One of the specimens was conventional SCBF (Specimen S0), and the other specimens are the SCBF with strongback columns. The selection of strongback columns was determined based on the results of numerical simulations. Because the results of DCF (Fig. 3) show that (α=0.0168, β=0.081) is the most suitable combination considering both effectiveness and cost, we use such combination for Specimen S73 where 7 denotes that the flexural stiffness of the strongback column is 7 times that of the column in the frame, and 3 denotes that the flexural strength of the strongback column is 3 times that of the column in the frame. The other specimen (S42) was expected to show moderate effects on reducing DCF; the corresponding (α, β) are (α=0.0096, β=0.054). The resulting size of the strongback column was RH346×174×6×9 for Specimen S73 and RH298×149×5.5×8 for Specimen S42. The whole specimens were composed of steels with the material properties shown in Table 2. The materials were STKR400 for the braces and SN490B for beams, columns, gussets and the rest parts of the specimens.

Table 2 Stress properties of materials

Structural Parts		*Fy*(MPa)	*Fu*(MPa)
Gusset		385	515
Column(RH150×150×7×10)		453	572
1F-Beam (RH198×99×4.5×7)		387	492
2F-Beam(RH194×150×6×9)		442	500
3F-Beam(RH300×150×6.5×9)		423	508
Brace		337	366
Strongback	RH346×174×6×9 (for S73)	506	603
	RH298×149×5.5×8 (for S42)	379	508

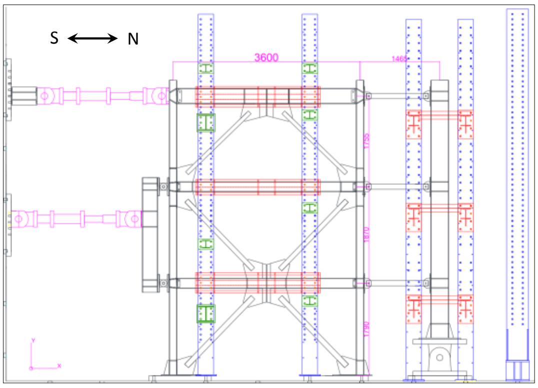

Fig. 4 Scheme of the test setup

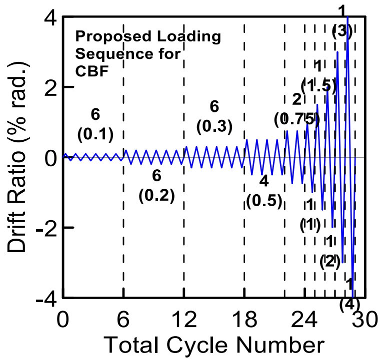

Loading Sequence for SCBF	
Roof Drift Ratio	Number of Cycles
0.1%	6
0.2%	6
0.3%	6
0.5%	4
0.75%	2
1%	1
1.5%	1
2%	1
3%	1
4%	1

Fig. 5 Loading sequence (Chen and Hu 2016)

3. Test program

Fig. 4 shows the test setup of the specimens. Continuous lateral supports were provided on the floor levels between the locations of the lateral-support columns. Another set of lateral support was provided for the strongback column to ensure the effects of strongback. The strongback column connected to the SCBF through simple links with pin ends on each floor. Also, the base of the strongback column was designed as a pin. As such, the strongback column did not provide lateral stiffness to the original SCBF when the deformation along the height is uniform; with such design, strongback column did not change the structural period significantly but provided corrective lateral forces at the onset of soft-story response.

Two actuators were used to apply lateral force and displacement to the specimens. We used the displacement-control method to give a specified loading sequence to the actuator on the top. Fig. 5 shows the loading sequence (Chen and Hu 2016) in this study varying from drift ratio = 0.1% rad. to 4% rad. The actuator on the bottom was force-controlled to follow the force of the top actuator, i.e. the forces of the top and bottom actuators were identical for each loading step. The force of the bottom actuator applied to the specimens through a transferring beam where the actuator was attached at 1/3 length from the top and the location of the pin supports was at the floor level of the 1st and the 2nd story. Therefore, the forces applied to the floor levels of three stories were in the proportion of 3:2:1, which is similar to the first mode shape of the three-story SCBF with equal mass and regular geometry in each story.

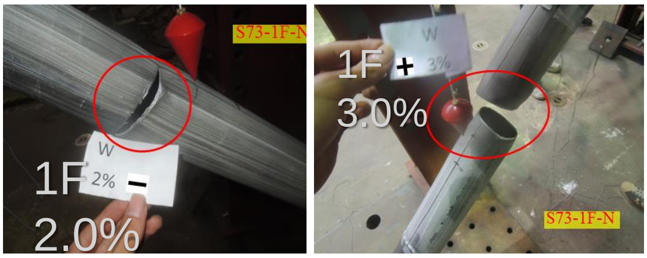

(a) (b)

Fig. 6 Damage of the brace in the 1st story in Specimen S73

4. Test results

4.1 Experimental observations

The tests are conducted in the Structural Lab of National Chiao Tung University in Taiwan. Both qualitative and quantitative data were recorded during tests. Specimen S73 was tested first followed by Specimen S42 and S0 to minimize the accumulation of damage to the beams, columns, and connections of the braced frame. Before replacing the damaged braces and proceeding to the next test, we reduced the roof residual displacement to less than 4 mm to minimize the geometric differences between specimens. Table 3 to Table 5 summarized some of the important events during the tests. Generally, the overall buckling of the braces in the 1st story took place at the roof drift ratio of 0.5% rad. for all the three specimens. The maximum base shears of all specimens were similar (about 600 kN). This demonstrated that the strongback column had only little effects on the maximum base shear.

For Specimen S73, the overall buckling of the braces in both the 2nd and 3rd story took place at the roof drift ratio=0.75% rad. In other words, all the three stories in Specimen S73 underwent nonlinear behavior after roof drift ratio=0.75% rad. Also, local buckling occurred after roof drift ratio=0.75% rad. Although severe crack of the brace in the 1st story was observed at roof drift ratio=2% rad. (Fig. 6 (a)), it ruptured at the roof drift ratio=3% rad (Fig. 6(b)).

For Specimen S42, the overall buckling of the braces in the 2nd story took place at the roof drift ratio=0.75% rad. and those in the 3rd story took place at the roof drift ratio=1% rad. The weaker and softer strongback column delayed the nonlinear behavior of the braces in the 3rd story. This implies that the material use is less efficient and the dissipated energy of the system is much less than its capacity. More important, this implies more drift concentration in the 1st and 2nd story. At the end of the test, the brace in the 1st story ruptured at the roof drift ratio=2% rad.

For Specimen S0, the overall buckling of the braces in the 2nd story took place at the roof drift ratio=0.75% rad. and those in the 3rd story took place at the roof drift ratio=1.5% rad. In the end of the test, the brace in the 1st story ruptured at the roof drift ratio=2% rad. The braces in the 3rd story did not participate in dissipating energy very much before the test stopped. This specimen showed typical weak-story mechanism of double-story X braced frame. Most of the deformation concentrates in the 1st and 2nd

Table 3 Critical events observed during the test of Specimen S73

Roof drift Ratio (rad.)	Critical Events
0.3%	* Flake of paint in the gusset near the beam-column connection in the 2nd story.
0.5%	* Overall buckling of both braces in the 1st story.
0.75%	* Local buckling of the northern brace close to the column base in the 1st story. * Overall buckling of braces in the 2nd and 3rd story.
1%	* Local buckling in the mid-length of both braces in the 1st story. * Local buckling of the southern brace close to the column base in the 1st story.
1.5%	* Surface crack in the mid-length of the southern brace in the 1st story. * Local buckling in the mid-length of both braces in the 2nd story. * Local buckling of both braces close to the beam-column connections in the 2nd story. * Local buckling of the southern brace close to the lower beam in the 2nd story.
2%	* Large crack in the mid-length of both braces in the 1st story. * Surface crack of the northern brace close to the column base in the 1st story. * Local buckling in the mid-length of both braces in the 3rd story. * Local buckling of both braces close to the beam-column connections in the 3rd story.
3%	* Rupture in the mid-length of both braces in the 1st story. * Local buckling of southern column flange in the 1st story * Large crack in the mid-length of the northern brace in the 2nd story. * Surface crack of both braces close to the beam-column connections in the 2nd story. * Flake of paint in beam webs and flanges in the beam-column connections in the 1st story.

Table 4 Critical events observed during the test of Specimen S42

Roof drift Ratio (rad.)	Critical Events
0.5%	* Flake of paint in southern column flange in the beam-column connection in the 1st story. * Overall buckling of both braces in the 1st story.
0.75%	* Local buckling in the mid-length of both braces in the 1st story. * Local buckling of both braces close to the column base in the 1st story. * Overall buckling of braces in the 2nd story. * Flake of paint in the flange of strongback column in the 3rd story.
1%	* Overall buckling of braces in the 3rd story.
1.5%	* Surface crack in the mid-length of both braces in the 1st story. * Surface crack of the northern brace close to the column base in the 1st story. * Local buckling in the mid-length of both braces in the 2nd story. * Local buckling of the southern brace close to the lower beam in the 2nd story.
2%	* Rupture in the mid-length of both braces in the 1st story.

Table 5 Critical events observed during the test of Specimen S0

Roof drift Ratio (rad.)	Critical Events
0.5%	* Overall buckling of both braces in the 1st story.
0.75%	* Local buckling in the mid-length of the southern brace in the 1st story. * Overall buckling of braces in the 2nd story.
1%	* Local buckling in the mid-length of the northern brace in the 1st story. * Flake of paint in the column flange in the beam-column connection in the 1st story.
1.5%	* Surface crack in the mid-length of both braces in the 1st story. * Surface crack of the northern brace close to the column base in the 1st story. * Local buckling in the mid-length of the southern brace in the 2nd story. * Local buckling of both braces close to the beam-column connections in the 2nd story. * Overall buckling of the northern brace in the 3rd story.
2%	* Rupture in the mid-length of both braces in the 1st story. * Local buckling in the mid-length of the northern brace in the 2nd story. * Overall buckling of the southern brace in the 3rd story.

story, and, therefore, the force and deformation demands in the braces of the 1st and 2nd story are greater than those of the specimens with the strongback column.

The critical events discussed previously are based on roof drift ratios; the corresponding drift ratios of brace buckling are compared in Table 6. Noted that the overall buckling is affected more by slenderness ratio of braces, and local buckling is affected more by compactness ratio of the brace sections. The overall buckling occurred at drift ratios ranging from 0.56% to 0.73% rad. and the local buckling occurred at drift ratios ranging from 0.89% to 1.11% rad. for the braces in the 1st story and 1.64% to 1.68% rad. for the braces in the 2nd and the 3rd story.

4.2 Quantitative investigation

Table 6 The drift ratios where the braces buckled

Specimen		Overall Buckle		Local Buckle		Test Stop
		Roof DR (rad)	Corresponding Story Drift (rad)	Roof DR (rad)	Corresponding Story Drift (rad)	Roof DR (rad)
S73	1F	+0.5%	+0.56%	+0.75%	+0.89%	3%
	2F	+0.75%	+0.73%	+1.5%	+1.64 %	
	3F	+0.75%	+0.64%	+2%	+1.67%	
S42	1F	+0.5%	+0.63%	+0.75%	+1.11%	2%
	2F	+0.75%	+0.66%	+1.5%	+1.65%	
	3F	+1%	+0.58%	N.A.	N.A.	
S0	1F	+0.5%	+0.62%	+0.75%	+1.07%	2%
	2F	+0.75	+0.58%	-1.5%	-1.68%	
	3F	-1.5%	-0.71%	N.A.	N.A.	

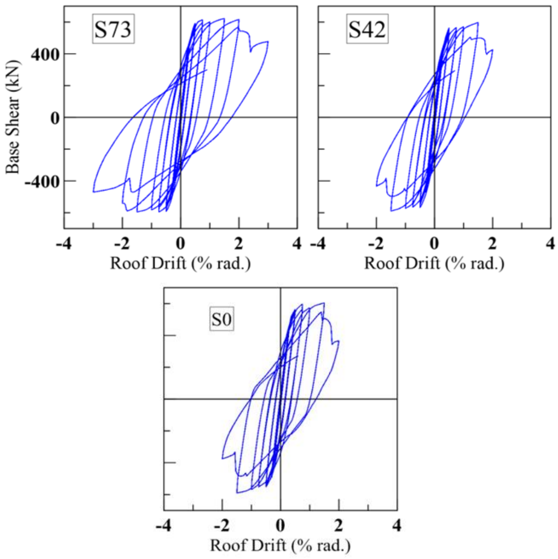

Fig. 7 The relationship between the base shear and the roof drift ratio of all specimens

4.2.1 Hysteretic behavior

Fig. 7 shows the relationship between the base shear and the roof drift ratio. For Specimen S73, the maximum base shear is 622 kN and maximum roof drift is 162.5 mm (DR=3%); for Specimen S42, the maximum base shear is 596 kN and maximum roof drift is 108.3mm (DR=2%); for Specimen S0, the maximum base shear is 603kN and maximum roof drift is 108.3 mm (DR=2%). The maximum base shear of the specimens was not affected by the presence of the strongback column because the strongback column only provided the capacity to redistribute the forces due to non-uniform deformation along the height of the building. The maximum roof drift of Specimen S73 increased because the deformation of the 3rd story increased, significantly. The nonlinear behavior began once the braces in the 1st story buckled. Near the end of the tests, the base shear dropped suddenly when the crack or rupture of the braces occurred. It usually initiated in the last cycle of the tests. Fig. 8 shows the relationship between the story shear and the story drift. It is convenient to compare the dissipated energy of each story visually. The dissipated energy in all the three stories of Specimen S73 is greater than that of other specimens. The nonlinear behavior was developed in the 3rd story of Specimen S42 and S73 and contributed to the total energy dissipation of the system. Moreover, the rupture of the brace in the 1st story delayed in Specimen S73, so the total cumulative energy is the greatest among the specimens. The brace rupture in the 1st story

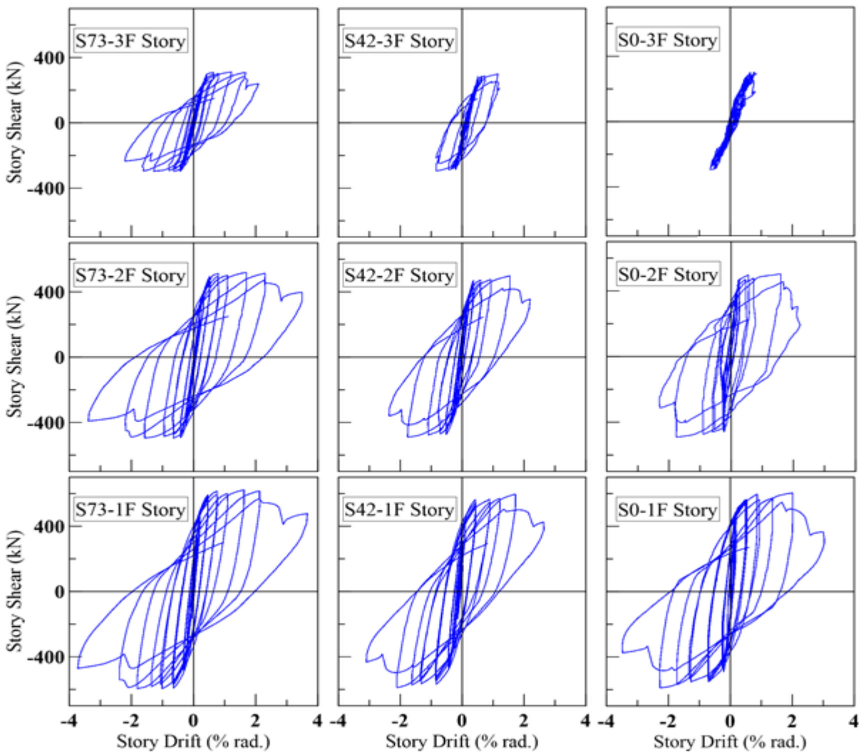

Fig. 8 The relationship between the story shear and the story drift ratio of all specimens

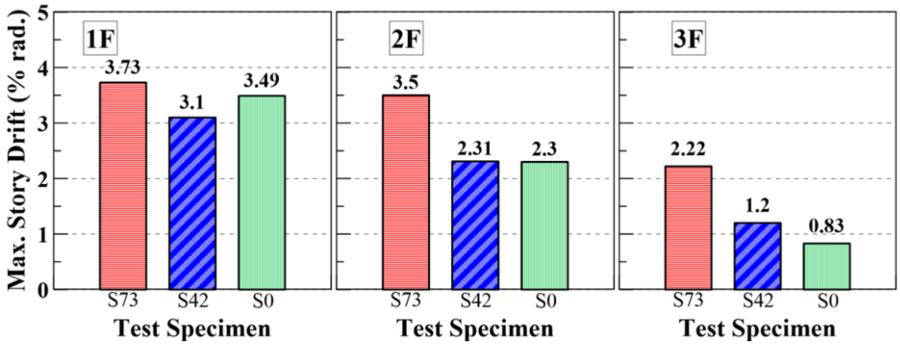

Fig. 9 Maximum story drifts of all specimens

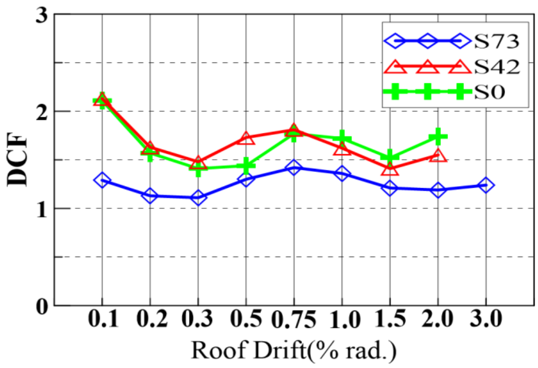

Fig. 10 Drift concentration factors under different roof drift ratios of all specimens

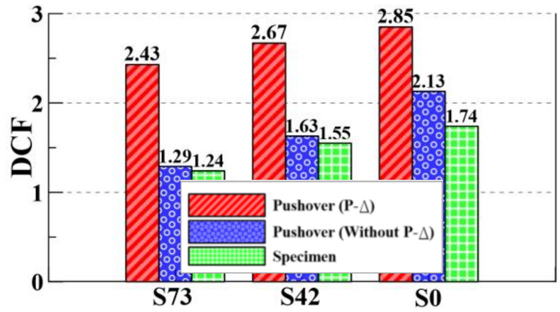

Fig. 11 Drift concentration factors of the specimens and the numerical models

delayed because the deformation demand in the 1st story was reduced; at the same roof drift ratio, Specimen S73 showed less drift ratio in the 1st story than the other specimens. The strongback column took effect to redistribute the deformation along the whole building and hence to reduce the drift ratio in the 1st story and delayed the rupture of the braces. The maximum story drifts of all specimens are compared in Fig. 9. For all the specimens, the maximum drift ratios in the 1st story are all greater than 3.0% rad. (3.73% for S73, 3.10% for S42, and 3.49% for S0). The major differences between specimens are the hysteretic behaviors of the 2nd and 3rd story. Specimen S73 is the only specimen where the maximum drift ratio in the 2nd story is greater than 3% rad. (3.50%), and the maximum drift ratio in the 3rd story is greater than 2% rad. (2.22%). The energy dissipation in the 3rd story of Specimen S73 is much greater than that of the other specimens. For Specimen S0, the response of the 3rd story even remains essentially elastic. Among all specimens, under the same roof drift, Specimen S73 shows the smallest story drift in the 1st story and the largest story drift in the 3rd story. It is obvious that the strongback column effectively changes the deformation along the height to a more uniform pattern, reduces the deformation demands in the 1st story, and increases the participation of the structural components in the 3rd story to dissipate energy.

4.2.2 Drift concentration factor

Drift concentration factor is used to identify the effectiveness of the strongback column to improve the system behavior. Under dynamic loading, DCF varies depending on the intensity of ground motions. Although the tests in this study were conducted with static cyclic loading, DCF also varied with the amplitude of applied displacement. Fig. 10 shows the DCF of all the specimens with respect to the roof drift ratio. Before the braces buckled, the specimens remained elastic and the deformation was small. For such cases, the DCF was amplified with the small roof drift ratio. However, such DCF was not associated with severe damage to the building. It is the large DCF with large roof drift ratio that leads to severe damage. For roof drift ratio greater than 0.75%, Specimen S0 shows the largest DCF, followed by Specimen S42 and S73. At the end of the tests, the DCF of Specimen S73 is 29% lower than that of Specimen S0 and the DCF of Specimen S42 is 11% lower than that of Specimen S0. Although Specimen S73 and S42 demonstrated satisfactory results for reducing DCF, the test results were different from the results of static pushover analysis. This was because of the P-Δ effect. The numerical simulations considered P-Δ effect with a leaning column. However, in the tests, the gravity load of the specimens only came from the self-weight of the bare frame. The test specimens were likely to perform better than the numerical models in terms of the DCF because of lighter gravity load. Fig. 11 compares the DCFs of Specimen S73, S42 and S0 with those of numerical counterparts. Such results illustrated the capability and accuracy of the numerical models.

4.2.3 Shear contributions from strongback

To investigate the shear contributions of the strongback column to the horizontal resistant of a certain story, we calculated the shear forces in the strongback column and compared them with the story shear. The shear forces of the

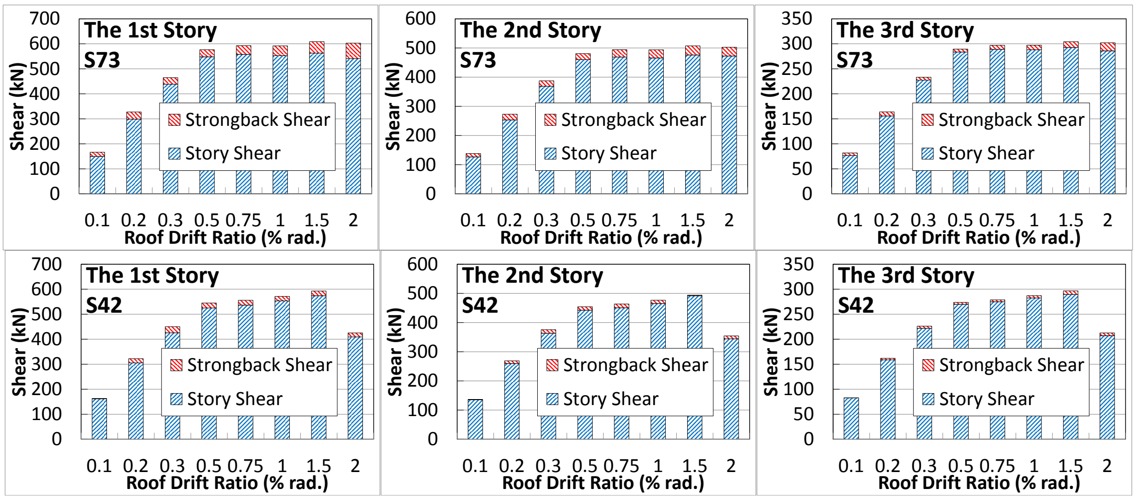

Fig. 12 The proportions of shear in the strongback column and SCBF for Specimen S73 and S42 under different roof drift ratios

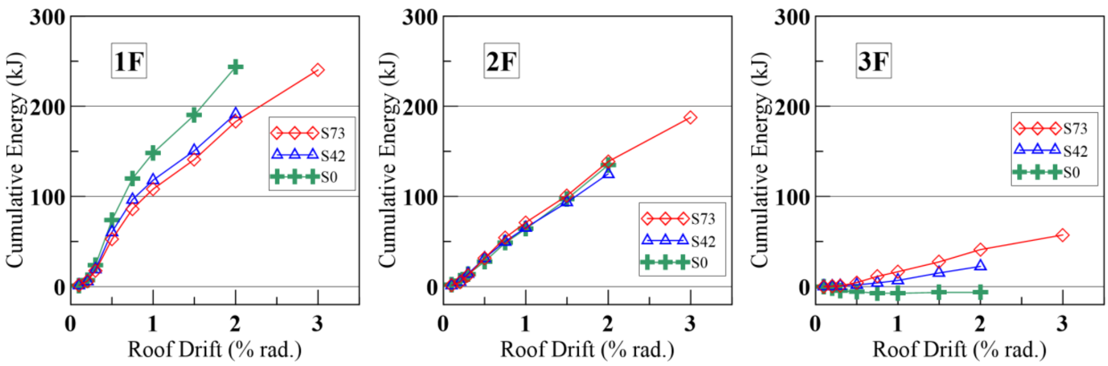

Fig. 13 The cumulative energy in each story for all specimens

strongback column were calculated by analyzing the strain data in the simple link, which connected the frame with the strongback column. The story shear of each story was calculated from the feedback force in the actuators. Fig. 12 shows the proportions of shear in the strongback column and SCBF at various roof drift ratios for Specimen S73 and S42. The general trend shows that the shear contribution of the strongback column is the greatest in the 1st story and the smallest in the 3rd story. For Specimen S73, the shear contribution of the strongback column in the 1st story is about 10%, which is greater than that for Specimen S42 (about 5%). Under small roof drift ratios, because the deformation of the system is relatively uniform, the effects of the strongback column are little. For example, the story shear of Specimen S42 at roof drift ratio of 0.1% was contributed mainly from the SCBF. After the braces buckled in the 1st story of both specimens (roof drift ratio = 0.5% rad.), the shear contributions of the strongback columns in the 1st story rise. The strongback columns were designed with limited strength capacity. The shear contributions of the strongback columns were roughly their capacity when the soft-story mechanism was developed under larger roof drift ratios. In general, the strongback columns were able to develop nonlinear behavior with stable cyclic performance. Only very minor damages, such as yielding in local regions, were observed in the strongback columns.

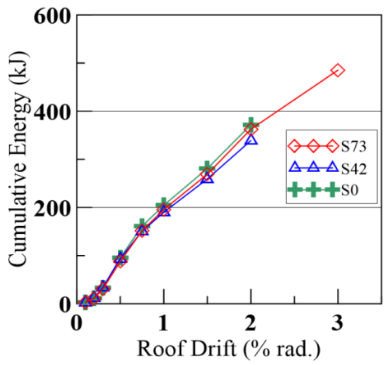

Fig. 14 The total cumulative energy for all specimens

4.2.4 Energy dissipation

Comparing the dissipated energy of the specimens is convenient to investigate their energy capacity. Fig. 13 shows the relationship between the cumulative energy of each story and the roof drift ratio. The cumulative energy was calculated based on the story shear and the story deformation. For the responses of the 1st story, because the force and deformation demands of Specimen S0 are greater than those of other specimens, the energy accumulation rate in the 1st story is also greater. For the responses of the 2nd story, the energy accumulation rates of all specimens are similar. More difference can be observed for the responses of the 3rd story; the energy accumulation rate and cumulative energy of Specimen S73 are much greater than those of other specimens under the same roof drift. The cumulative energy of Specimen S0 in the 3rd story is even close to zero representing essentially elastic response. The negative values were the measuring errors from string pot. The cumulative energy in the 1st story is associated with the ductility capacity of the braces. For Specimen S73, the strongback column effectively made more deformation occur in other stories before the braces in the 1st story reached their ductility capacity, and, therefore, increased the total dissipated energy of the system. Fig. 14 compares the total cumulative energy of all specimens with respect to the roof drift ratio. The energy accumulation rates of all specimens are similar, but Specimen S73 shows the best capacity of energy dissipation; Specimen S73 dissipated 30% more energy than Specimen S42 and S0. Such results also illustrate that Specimen S73 with the help of the strongback column has better deformation capacity in terms of roof drift, potentially greater energy dissipation capacity and more efficient use of materials. On the other hand, for Specimen S42, although the DCF was effectively reduced, its strongback column did not help increase the energy capacity of the whole system, significantly.

5. Conclusions

To investigate the effects of the strongback on SCBF, we tested three 1/3 scaled specimens. The specimens were designed according to the results of numerical simulations. Two of them were the specimens with the strongback column of different strength and stiffness. According to the test results, the conclusions were made.

- Properly designed strongback columns effectively redistribute the deformation of structure uniformly along the height and reduce the DCF of the building. The DCF of Specimen S73 is 29% lower than that of Specimen S0 and the DCF of Specimen S42 is 11% lower than that of Specimen S0.
- Strongback in Specimen S73 was able to postpone the rupture of braces in the 1st story. The braces rupture at 3% roof drift ratio for Specimen S73 and 2% for Specimen S42 and S0. It is noted that the maximum drift ratios of Specimen S73 and S0 in the 1st story are similar.
- Test results were consistent with the numerical results of the model without considering P-Δ effects. In real practice, we suggest that P-Δ effects should be considered although such consideration may result in less reduction in DCF. The strongback column is still very likely to increase the energy dissipation capacity of the system by a large amount.
- The shear contribution of the strongback column is about 5% of the total story shear. Also, such shear demands of the strongback column increase when more drift concentration tends to occur.
- The strongback column in Specimen S73 effectively reduces the force and deformation demands in the 1st story and, in the meantime, increases those in the 3rd story. Such effects result in a better seismic performance of SCBF. Specimen S73 dissipated 30% more energy than Specimen S42 and S0. The strongback column of Specimen S42, on the other hand, is less effective in terms of energy dissipation capacity of the system.

Acknowledgments

This work was supported by the Ministry of Science and Technology under the Grants 103-2625-M-009-011. The authors would like to thank Prof. Stephen Mahin for sharing the pioneering concept of strongback and inspiring the numerical and experimental investigations on the system. The technical support from National Center for Research on Earthquake Engineering and Dr. Kung-Juin Wang are also appreciated.

References

ANSI/AISC 341-10 (2010), Seismic Provisions for Structural Steel Buildings, American Institute of Steel Construction, Chicago, IL.

Chen, C.H. and Hu, H.K. (2016), “Evaluation of loading sequences on testing capacity of concentrically braced frame structures”, *J. Constr. Steel Res.*, **130**(1), 1-11. https://doi.org/10.1016/j.jcsr.2016.11.017.

Chen, C.H. and Mahin, S. (2012), “Performance-based seismic demand assessment of concentrically braced steel frame buildings”, PEER-2012/103, Pacific Earthquake Engineering Research Center, University of California, Berkeley, CA.

Chen, C.H., Tsia, I.J. and Tang, Y. (2016), “Drift concentration of a three-story special concentrically braced frame with strongback under earthquake loading”, *Appl. Mech. Mater.*, **863**, 287-292.
https://doi.org/10.4028/www.scientific.net/AMM.863.287.

DASSE (2007), *Cost Advantages of Buckling Restrained Braced Frame Buildings*, DASSE Design Inc.

Eskandari, R., Vafaei, D., Vafaei, J. and Shemshadian, M.E. (2017), “Nonlinear static and dynamic behavior of reinforced concrete steel-braced frames”, *Earthq. Struct.*, **12**(2), 191-200. https://doi.org/10.12989/eas.2017.12.2.191.

Güneyisi, E.M. and Azez, I. (2016), “Seismic upgrading of structures with different retrofitting methods”, *Earthq. Struct.*, **10**(3), 589-611. https://doi.org/10.12989/eas.2016.10.3.589.

Ji, X., Kato, M., Wang, T, Hitaka, T. and Nakashima, M. (2009), “Effect of gravity columns on mitigation of drift concentration for braced frames”, *J. Constr. Steel Res.*, **65**, 2148-2156. https://doi.org/10.1016/j.jcsr.2009.07.003.

Khatib, F., Mahin, S. and Pister, K.S. (1988), “Seismic behavior of concentrically braced steel frames”, UCB/EERC-88/01, Earthquake Engineering Research Center, University of California, Berkeley, CA.

Lai, J.W. and Mahin, S. (2013), “Experimental and analytical studies on the seismic behavior of conventional and hybrid braced frames”, PEER-2013-20, Pacific Earthquake Engineering Research Center, University of California, Berkeley, CA.

MacRae, G.A., Kimura, Y. and Roeder, C.W. (2004), “Effect of column stiffness on braced frame seismic behavior”, *J. Struct. Eng.*, ASCE, **130**(3), 381-391. https://doi.org/10.1061/(ASCE)0733-9445(2004)130:3(381).

Mar, D. (2010), “Design examples using mode shaping spines for frame and wall buildings”, *Proceedings of the 9th U.S. National and 10th Canadian Conference on Earthquake Engineering*,

Paper No. 1400, Toronto, Canada.
McKenna, F. (1997), *Object Oriented Finite Element Programming: Frameworks for Analysis*, Algorithms and Parallel Computing, University of California, Berkeley, CA.
Pollino, M., Slovenec, D., Qu, B. and Mosqueda, G. (2017), "Seismic rehabilitation design and analysis of concentrically braced frames using stiff elastic cores", *J. Struct. Eng.*, ASCE, **143**(9), 04017080. https://doi.org/10.1061/(ASCE)ST.1943-541X.0001810.
Qu, B., Sanchez-Zamora, F. and Pollino, M. (2014), "Mitigation of inter-story drift concentration in multi-story steel concentrically braced frames through implementation of rocking cores", *Eng. Struct.*, **70**, 208-217. https://doi.org/10.1016/j.engstruct.2014.03.032.
Qu, B., Sanchez-Zamora, F. and Pollino, M. (2015), "Transforming seismic performance of deficient steel concentrically braced frames through implementation of rocking cores", *J. Struct. Eng.*, ASCE, **141**(5), 04014139. https://doi.org/10.1061/(ASCE)ST.1943-541X.0001085.
Qu, B., Sanchez-Zamora, F., Pollino, M. and Hou, M.H. (2016), "Rehabilitation of steel concentrically braced frames with rocking cores for improved performance under near-fault ground motions", *Adv. Struct. Eng.*, **20**(6), 940-952. https://doi.org/10.1177/1369433216668101.
Qu, Z., Wada, A. Motoyui, S., Sakata, H. and Kishiki, S. (2012) "Pin-supported walls for enhancing the seismic performance of building structures", *Earthq. Eng. Struct. Dyn*., **41**, 2075-2091. https://doi.org/10.1002/eqe.2175.
Sabelli, R. (2001), "Research on improving the design and analysis of earthquake-resistant steel-vraced frames", Earthquake Engineering Research Institute, the 2000 NEHRP Professional Fellowship Report, PF2000-9, Oakland, CA.
Simpson, B.G. and Mahin, S.A. (2018) "Experimental and numerical investigation of strongback braced frame system to mitigate weak story behavior", *J. Struct. Eng.*, ASCE, **144**(2), 04017211. https://doi.org/10.1061/(ASCE)ST.1943-541X.0001960.
Slovenec, D., Sarebanha, A., Pollino, M., Mosqueda, G. and Qu, B. (2017), "Hybrid testing of the stiff rocking core seismic rehabilitation technique", *J. Struct. Eng.*, ASCE, **143**(9), 04017083. https://doi.org/10.1061/(ASCE)ST.1943-541X.0001814.
Somerville, P.G. (1997), Development of Ground Motion Time Histories for Phase 2 of the FEMA /SAC Steel Project, SAC BD/97-04, SAC Steel Joint Venture, Sacramento California.
Tehranizadeh, M., Amirmojahedi, M. and Moshref, A. (2016), "Simplified methods for seismic assessment of existing buildings", *Earthq. Struct.*, **10**(6), 1405-1428. http://dx.doi.org/10.12989/eas.2016.10.6.1405.
Tirca, L. and Tremblay, R. (2004), "Influence of building height and ground motion type on the seismic behavior of zipper concentrically braced steel frames", *Proceedings of the 13th World Conference on Earthquake Engineering*, Paper No. 2894, Vancouver, B.C., Canada.
Tremblay, R. (2003), "Achieving a stable inelastic seismic response for multi-story concentrically braced steel frames", *Engineering Journal*, Second Quarter.
Tremblay, R. and Merzouq, S. (2004), "Dual buckling restrained braced steel frames for enhanced seismic response", *Proceedings of Passive Control Symposium*, Yokohama, Japan.
Uriz, P. and Mahin, S. (2008), *Towards Earthquake Resistant Design of Concentrically Braced Steel Structures*, PEER-2008/08, Pacific Earthquake Engineering Research Center, University of California, Berkeley, CA.
Wada, A., Qu, Z., Motoyui, S. and Sakata, H. (2011), "Seismic retrofit of existing SRC frames using rocking walls and steel dampers", *Front. Arch. Civil Eng.*, **5**(3), 259-266. https://doi.org/10.1007/s11709-011-0114-x.

KT